Intensity-dependent enhancements in high-order above-threshold ionization

D. B. Milošević,[1,2] E. Hasović,[1] M. Busuladžić,[3] A. Gazibegović-Busuladžić,[1] and W. Becker[2]
[1]*Faculty of Science, University of Sarajevo, Zmaja od Bosne 35, 71000 Sarajevo, Bosnia and Herzegovina*
[2]*Max-Born-Institut, Max-Born-Strasse 2a, 12489 Berlin, Germany*
[3]*Medical Faculty, University of Sarajevo, Čekaluša 90, 71000 Sarajevo, Bosnia and Herzegovina*
(Received 15 August 2007; published 14 November 2007)

The very pronounced intensity-dependent enhancements of groups of peaks of high-order above-threshold-ionization spectra of rare-gas atoms are investigated using an improved version of the strong-field approximation, which realistically models the respective atom. Two types of enhancements are found and explained in terms of constructive interference of the contributions of a large number of long quantum orbits. The first type is observed for intensities slightly below channel closings. Its intensity dependence is comparatively smooth and it is generated by comparatively few (of the order of 20) orbits. The second type occurs precisely at channel closings and exhibits an extremely sharp intensity dependence. It requires constructive interference of a very large number of long orbits (several hundreds) and generates cusps in the electron spectrum at integer multiples of the laser-photon energy. An interpretation of these enhancements as a threshold phenomenon is also given. An interplay of different types of the threshold anomalies is observed. The position of both types of enhancements, in the photoelectron-energy—laser-intensity plane, shifts to the next channel closing intensity with the change of the ground-state parity. The enhancements gradually disappear with decreasing laser pulse duration. This confirms the interpretation of enhancements as a consequence of the interference of long strong-laser-field-induced quantum orbits.

DOI: 10.1103/PhysRevA.76.053410 PACS number(s): 32.80.Rm, 42.50.Hz, 32.80.Qk

I. INTRODUCTION

Above-threshold ionization (ATI) of atoms by intense laser radiation is a nonlinear quantum-mechanical phenomenon that is characterized by a sequence of peaks in the electron spectrum, spaced by the photon energy. Since its discovery [1], the interest in ATI has been renewed many times (for a review see [2–5]). In 1993 the sidelobes (scattering rings) in the angular distributions were discovered [6], and a plateau in the high-energy electron spectra, where the ionization probability is independent of the photoelectron's energy up to a rather well-defined cutoff, was observed [7,8]. The photoelectron energy spectra were explained by the rescattering or three-step model [6–10]. According to this model, photoelectrons can be separated into direct and rescattered electrons. After becoming free at some well-defined ionization time, direct electrons are not affected anymore by the binding potential. After the first few peaks (sometimes this region is called a first plateau), the spectrum decreases exponentially with increasing energy. Classically, their energy cannot exceed $2U_P$, where U_P is the ponderomotive energy. The electron can achieve much higher energies if, driven by the laser field, it revisits its parent ion and backscatters. In this event, it may be accelerated for another half period of the laser field and reach a kinetic energy of up to $10U_P$. Rescattered and backscattered electrons form a plateau whose yield is lower by several orders of magnitude than the yield of direct electrons. The transition from direct electrons to the plateau occurs at an energy of the order $2U_P$ or higher. Where exactly the transition takes place depends on the laser wavelength, laser intensity, and the atomic or ionic species. Especially, it was also shown that the energy at which the exponentially decreasing yield of the low-energy electrons intersects the yield of the rescattering-plateau electrons depends on the parity of the atomic ground state and can reach values above $4U_P$ [11]. A more recent semiclassical generalization of this three-step model gives the cutoff at $10.007U_P + 0.538I_P$ [12], where I_P is the ionization energy.

In 1997 resonantlike enhancements for particular laser intensities in high-energy ATI have been discovered in experiments with inert gases [13]. The observed photoelectron spectrum was composed of narrow individual peaks whose energy positions do not shift with the change of the laser-field intensity. In fact, depending on the inert gas used, separate series of peaks, each with a distinct intensity threshold for their onset, have been observed. More recent experiments have confirmed these resonantlike enhancements [14–16]. Furthermore, it was found that the enhancements become suppressed with the decrease of the laser pulse duration [17,18]. ATI by few-cycle pulses has become an important tool for attosecond physics: the ATI spectrum, notably its rescattering part, depends very sensitively on the carrier-envelope phase and has frequently been used for its control and stabilization [5,19–22].

It is not possible to explain the mentioned enhancements using the classical three-step model: all elements of the latter, such as ionization rates, cutoffs, and classical orbits depend continuously and smoothly on the laser intensity, providing no mechanism for a sudden surge of any feature as a function of intensity. Hence it appears that a quantum treatment is required. At present, there is no consensus about the physical origin of these resonantlike enhancements. The various quantum-mechanical approaches to their theoretical interpretation can be divided into two groups. The first is based on an analysis of the numerical solution of the time-dependent Schrödinger equation [23,24] or on an analysis of the Floquet quasienergy spectrum [25,26]. According to these findings, the enhancements occur at particular intensities where the atom is in a state that is a superposition of the

laser-dressed ground state and of one or several laser-dressed excited states. For Coulomb-like potentials, besides the ground state there are many excited (Rydberg) states and the enhancements are related to multiphoton resonances with these states. For short-range potentials (for example, for the zero-range potential) there is only a single bound state. In this case, it was suggested that light-induced states [27,28], which lie very close to the continuum threshold, take over the role of Rydberg states and allow a similar interpretation of the enhancements [25].

The second group of approaches does not require any excited states. It attributes the resonantlike enhancements to the well-known channel closings (CCs), which occur when the laser intensity increases. After it has left the field, the kinetic energy of an electron generated by ionization is

$$E_{\mathbf{p}} \equiv \frac{\mathbf{p}^2}{2m} = n\hbar\omega - I_{\mathrm{P}} - U_{\mathrm{P}}, \tag{1}$$

where $\mathbf{p}$ denotes its momentum, I_{P} the ionization energy of the respective atom, and ω the frequency of the laser field. Ionization is made possible because the laser field "provides n photons." The lowest energy that the freed electron can have is $E_{\mathbf{p}}=0$. The ponderomotive energy U_{P} is proportional to the intensity of the laser field. Hence when the latter increases, at some intensity I_{c}, absorption of n_{c} photons no longer suffices for ionization, and $n_{\mathrm{c}}+1$ photons are required; we say that the n_{c}-photon channel has closed. This intensity is given by

$$U_{\mathrm{Pc}} + I_{\mathrm{P}} = n_{\mathrm{c}}\hbar\omega, \tag{2}$$

where U_{Pc} denotes the corresponding ponderomotive energy. Electrons born by ionization at this intensity have energies

$$E_{\mathbf{p}} = k\hbar\omega \tag{3}$$

with integer $k \geqslant 0$. This spectrum includes electrons with zero drift energies. They are driven by the laser field (if one disregards the atomic Coulomb field) into an infinite series of recollisions with the ion. Calculations show that near the intensity I_{c} the yields of a group or several groups of ATI peaks within the rescattering plateau are raised significantly, by up to an order of magnitude [16,29].

There are two complementary interpretations of why a CC leads to an enhancement. The first is based on the semiclassical generalization of the three-step model. As mentioned above, near a CC an ionized electron is driven by the field into multiple recollisions with its parent ion. Upon each recollision, the electron may rescatter. If all of the corresponding contributions to the ionization amplitude interfere constructively, a very substantial enhancement results [16,29]. It was shown analytically within the strong-field approximation that the conditions for constructive interference are satisfied near a CC [30]. Note that each individual contribution is well described classically, but the concept of their constructive interference is quantum-mechanical. The absence of resonantlike enhancements in the ATI plateau in experiments with short laser pulses [17] supports the above theoretical explanation that constructive interference of the contributions of many long trajectories is responsible for the CC enhancements. This interpretation can be cast more precisely in terms of Feynman's path integral and quantum-orbit theory [3,5,16,21,29–37]. It will be the main subject of the present paper.

The second interpretation treats the enhancements as an example of well-known threshold phenomena [38–40] in the case where a multiphoton channel closes. That is, it regards the enhancements as a manifestation of the threshold anomalies of collision theory [41–43] for the case of multiphoton processes [44]. This interpretation has been introduced in the context of calculations of above-threshold detachment of negative ions, based on the zero-range potential model [45]. More recently, for negative ions with p ground states, an effective-range model was introduced [46]. It was found that the enhancement effects strongly depend on the orbital angular momentum l of the bound electron [47]. For even (odd) l the enhancement is most pronounced for even (odd) CCs. Similar conclusions were obtained in [48] (see also [49] for an earlier report about these findings) by solving the time-dependent Schrödinger equation within the Sturmian-Floquet approach.

In the present paper we will further develop the quantum-orbit theory of high-order ATI and apply it to explain the CC enhancements. Particular attention will be devoted to the influence of the parity of the initial bound state, in order to show that quantum-orbit theory can also explain the findings of Refs. [47–49]. Our paper is organized as follows. We introduce our theory in Sec. II. We first define the ionization probability amplitude and the differential ionization rate and then we introduce the improved strong-field approximation (SFA), which includes the rescattering of the ionized electron off its parent ion. Next, we present the saddle-point approximation and introduce a classification of the saddle-point solutions. Section II concludes with a numerical example based on the uniform approximation, which is more precise than the saddle-point approximation. In Sec. III a semiclassical cutoff law is presented and analyzed in terms of the saddle-point solutions. In Sec. IV we derive the conditions for the constructive interference of the partial T-matrix contributions, while in Sec. V we analyze high-order ATI enhancements in terms of long quantum orbits. In Sec. VI, we recognize the ATI enhancements as an example of the threshold anomalies known from scattering theory with inelastic channels. Section VII contains our numerical results which are based on the numerical integration of the improved SFA T-matrix element. We observe two very different manifestations of CCs in the ATI spectrum, which we classify as type-I and type-II enhancements. In Sec. VIII the possibility of observing these different types in the focal-averaged spectra is considered. In Sec. IX we show how these enhancements gradually disappear with decreasing laser pulse duration. Finally, our conclusions are given in Sec. X. We will use the atomic system of units ($\hbar=e=m=4\pi\varepsilon_0=1$).

II. THEORY

The probability amplitude for detecting an ATI electron with momentum $\mathbf{p}$ and kinetic energy $E_{\mathbf{p}} \equiv \mathbf{p}^2/2$, within the S-matrix approach, is [3,50]

$$M_{\mathbf{p}i} = -i \lim_{t\to\infty} \int_{-\infty}^{t} dt_0 \langle \psi_{\mathbf{p}}(t)|U(t,t_0)\mathbf{r}\cdot\mathbf{E}(t_0)|\psi_i(t_0)\rangle. \quad (4)$$

The states $|\psi_{\mathbf{p}}(t)\rangle$ and $|\psi_i(t)\rangle = |\psi_i\rangle \exp(iI_P t)$ are a scattering state with asymptotic momentum $\mathbf{p}$ and the initial atomic ground state, respectively, of the atomic Hamiltonian $H_i = -\nabla^2/2 + V(\mathbf{r})$, with $V(\mathbf{r})$ the interaction of the electron with the rest of the atom in the absence of the laser field. In Eq. (4), $U(t,t_0)$ is the time-evolution operator of the complete Hamiltonian $H(t) = H_i + \mathbf{r}\cdot\mathbf{E}(t)$, where $\mathbf{r}\cdot\mathbf{E}(t)$ is the laser-field-electron interaction in the length gauge and the dipole approximation, $\mathbf{E}(t) = -d\mathbf{A}(t)/dt$ is the electric field vector, and $\mathbf{A}(t)$ is a vector potential of the laser field.

A. Improved strong-field approximation

The time-evolution operator $U(t,t_0)$ satisfies the Dyson equation

$$U(t,t_0) = U_L(t,t_0) - i\int_{t_0}^{t} dt' U_L(t,t')V(\mathbf{r})U(t',t_0), \quad (5)$$

where $U_L(t,t_0) = \int d^3\mathbf{k} |\psi_{\mathbf{k}}^{(L)}(t)\rangle\langle\psi_{\mathbf{k}}^{(L)}(t_0)|$ is the Volkov time-evolution operator and

$$|\psi_{\mathbf{p}}^{(L)}(t)\rangle = |\mathbf{p} + \mathbf{A}(t)\rangle \exp[-iS_{\mathbf{p}}(t)] \quad (6)$$

are the Volkov states in length gauge. Here $|\mathbf{q}\rangle$ denotes a plane-wave state $[\langle \mathbf{r}|\mathbf{q}\rangle = (2\pi)^{-3/2}\exp(i\mathbf{q}\cdot\mathbf{r})]$, and

$$S_{\mathbf{p}}(t) = \frac{1}{2}\int^{t} dt' [\mathbf{p} + \mathbf{A}(t')]^2. \quad (7)$$

Inserting Eq. (5), with the operator $U(t,t_0)$ on the right-hand side approximated by $U_L(t,t_0)$, into Eq. (4), we obtain the transition amplitude in the improved strong-field approximation [11,51–55], which we present here in the form

$$M_{\mathbf{p}i}^{\mathrm{SFA}} = M_{\mathbf{p}i}^{(0)} + M_{\mathbf{p}i}^{(1)}, \quad (8)$$

where $M_{\mathbf{p}i}^{(0)} = M_{\mathbf{p}i}^{(0)}(\infty)$, with

$$M_{\mathbf{p}i}^{(0)}(t) = -i\int_{-\infty}^{t} dt_0 \langle \psi_{\mathbf{p}}^{(L)}(t_0)|\mathbf{r}\cdot\mathbf{E}(t_0)|\psi_i(t_0)\rangle, \quad (9)$$

and

$$M_{\mathbf{p}i}^{(1)} = \int_{-\infty}^{\infty} dt \int d^3\mathbf{k} M_{\mathbf{p}\mathbf{k}}^{(0)}(t) M_{\mathbf{k}i}^{(0)}(t), \quad (10)$$

with

$$M_{\mathbf{p}\mathbf{k}}^{(0)}(t) = -i\langle \psi_{\mathbf{p}}^{(L)}(t)|V(\mathbf{r})|\psi_{\mathbf{k}}^{(L)}(t)\rangle. \quad (11)$$

The term $M_{\mathbf{p}i}^{(0)}$ in Eq. (8) is the standard SFA (in its length-gauge version), which describes direct ATI, while $M_{\mathbf{p}i}^{(1)}$ is the rescattering amplitude, which is responsible for the high-energy plateau in the electron energy spectrum. Physically, the rescattering amplitude incorporates the three-step model of high-order ATI [3,4,10]. The electron is ionized at the time t_0 and propagates under the influence of only the laser field until the time t. These two steps are described by the amplitude $M_{\mathbf{k}i}^{(0)}(t)$, Eq. (9). At the time t, the electron, being in the Volkov state with the momentum $\mathbf{k}$, scatters elastically off the potential $V(\mathbf{r})$. After the laser-assisted scattering, described by the amplitude $M_{\mathbf{p}\mathbf{k}}^{(0)}(t)$, Eq. (11), the electron's final momentum at the detector is $\mathbf{p}$. In Eq. (10) we also have to integrate over all intermediate electron momenta $\mathbf{k}$ and over all rescattering times t.

For a periodic laser field with the period $T = 2\pi/\omega$, the transition amplitude can be decomposed in the form [4]

$$M_{\mathbf{p}i}^{(j)} = -2\pi i \sum_n \delta(E_{\mathbf{p}} + I_P + U_P - n\omega) T_{\mathbf{p}i}^{(j)}(n), \quad (12)$$

where $T_{\mathbf{p}i}^{(j)}(n)$, $j = 0, 1$, is the corresponding T-matrix element of the ATI process and U_P is the ponderomotive energy defined by the nonperiodic part of $\frac{1}{2}\int^t dt' \mathbf{A}^2(t') = \mathcal{U}_1(t) + U_P t$, with $\mathcal{U}_1(t+T) = \mathcal{U}_1(t)$. The argument of the δ function in Eq. (12) displays energy conservation in terms of "absorption of laser photons." The explicit forms of the SFA T-matrix elements $T_{\mathbf{p}i}^{(0)}(n)$ and $T_{\mathbf{p}i}^{(1)}(n)$, as well as the choice of the ground-state wave function ψ_i and the rescattering potentials $V(\mathbf{r})$ for the inert gases He, Ne, Ar, Kr, and Xe, are given in Ref. [11]. The differential ionization rate with absorption of n photons then is

$$w_{\mathbf{p}i}(n) = 2\pi p |T_{\mathbf{p}i}^{(0)}(n) + T_{\mathbf{p}i}^{(1)}(n)|^2, \quad (13)$$

where the additional factor 2π comes from the integration over all azimuthal angles ϕ of the momentum $\mathbf{p} = (p,\theta,\phi)$ of the emitted electron.

B. Saddle-point approximation

The matrix element in the integrand of Eq. (10) can be represented in the form $A_{\mathbf{p}i}\exp(iS_{\mathbf{p}i})$ where the action $S_{\mathbf{p}i}$ consists of three parts,

$$S_{\mathbf{p}i}(t,t_0,\mathbf{k}) = -\int_{t}^{\infty} dt' [\mathbf{p} + \mathbf{A}(t')]^2/2 - \int_{t_0}^{t} dt' [\mathbf{k} + \mathbf{A}(t')]^2/2 + I_P t_0, \quad (14)$$

in accordance with the three-step model discussed in Secs. I and II A. The integral over the intermediate electron momentum $\mathbf{k}$, which comes from the Volkov time-evolution operator, can be solved using the saddle-point method [3,4]. The action is stationary, i.e., $\nabla_{\mathbf{k}} S_{\mathbf{p}i}(t,t_0,\mathbf{k}) = \mathbf{0}$, for the momentum $\mathbf{k} = \mathbf{k}_s = -\int_{t_0}^{t} dt' \mathbf{A}(t')/(t-t_0)$. This condition corresponds to the requirement that the electron returns to its parent ion. The stationarity conditions with respect to the remaining two integration variables t_0 and t lead to the relations

$$[\mathbf{k}_s + \mathbf{A}(t_0)]^2 = -2I_P, \quad (15)$$

$$[\mathbf{k}_s + \mathbf{A}(t)]^2 = [\mathbf{p} + \mathbf{A}(t)]^2. \quad (16)$$

Physically, these two conditions correspond to energy conservation at the time t_0 of ionization and at the time t of rescattering. The above equations are the basis of the quantum-orbit theory [3,5,21,29–37]. Application of the

saddle-point method [56] to the double integral over the times t_0 and t leads to a sum over solutions $\{t_{0s}, t_s\}$ of the system (15) and (16). The corresponding T-matrix element, which appears in Eqs. (12) and (13), has the form

$$T_{\mathbf{p}i}^{(1)}(n) = \sum_s A_s e^{iS_s} = \omega \sum_s V_{\mathbf{k}_s - \mathbf{p}} \Delta_s^{-1/2} \langle \mathbf{k}_s + \mathbf{A}(t_{0s}) | \mathbf{r} \cdot \mathbf{E}(t_{0s}) | \psi_i \rangle \exp(iS_s), \tag{17}$$

where $V_{\mathbf{K}} = (2\pi)^{-3} \int d^3\mathbf{r} V(\mathbf{r}) \exp(i\mathbf{K}\cdot\mathbf{r})$, $S_s \equiv S(t_{0s}, t_s)$, and $\Delta_s \equiv \Delta(t_{0s}, t_s)$, with

$$S(t_0, t) = E_{\mathbf{p}} t + \mathbf{p} \cdot \boldsymbol{\alpha}(t) + E_{\mathbf{k}_s}(t - t_0) + (U_\mathrm{P} + I_\mathrm{P}) t_0 + \mathcal{U}_1(t_0), \tag{18}$$

$$\Delta(t_0, t) = \left[\frac{i(t - t_0)}{2\pi} \right]^3 \left[\left(\frac{\partial^2 S}{\partial t_0 \partial t} \right)^2 - \frac{\partial^2 S}{\partial t_0^2} \frac{\partial^2 S}{\partial t^2} \right]. \tag{19}$$

Here $\boldsymbol{\alpha}(t) = \int^t dt' \mathbf{A}(t')$ and $E_{\mathbf{p}} = n\omega - I_\mathrm{P} - U_\mathrm{P}$. We will call the result (17)–(19) the saddle-point approximation (SPA). An example of comparison of the ATI spectra obtained solving the time-dependent Schrödinger equation with the SPA results is presented in Ref. [37], while a comparison of the results obtained using the improved SFA with the SPA results is given in Ref. [11] and in Refs. [5,21] for few-cycle laser pulses.

The direct part of the spectrum can also be approximated by the saddle-point method. The corresponding saddle-point solutions of the one-dimensional integral (9) can be represented in analytical form. Here we concentrate on the rescattering part of the spectrum. The direct part is significantly modified by the effects of the Coulomb potential, which are not taken into account in the present theory.

C. Saddle-point solutions

For a linearly polarized laser field, the system (15) and (16) can be solved similarly as it has been done for high-order harmonic generation in Ref. [36]. The solutions $\{t_{0s}, t_s\}$ are characterized by a multiindex consisting of the three numbers $s \equiv \alpha\beta m$ [57]. This notation is explained in Fig. 1. We restrict the rescattering times t to one cycle of the field so that $0 \leqslant \mathrm{Re}\, t < T$. For each t there are infinitely many pairs of solutions, which can be ordered by their ionization time t_0. For $-(m+1/2)T \leqslant \mathrm{Re}\, t_0 < -(m-1/2)T$, where $m = 0, 1, 2, \ldots$, there are two pairs of solutions. The pair having the longer (shorter) travel time $\mathrm{Re}(t - t_0)$ carries the index $\beta = -1$ ($\beta = +1$). Each pair again consists of two orbits with slightly different travel times. This is well-known from the Lewenstein model [31] of high-order harmonic generation. We discriminate the longer from the shorter orbit by the index α as indicated in Fig. 1 [59]. The index m gives the approximate length of the travel time in multiples of the laser period, $m = [(t - t_0)/T]$ (with $[x]$ the largest integer $\leqslant x$). For $m = 0$, there is only one pair of solutions, having $\beta = -1$. For all solutions, the imaginary part of the variable $\varphi = \omega t$ is very small, while its real part lies in the interval $[0, 2\pi]$.

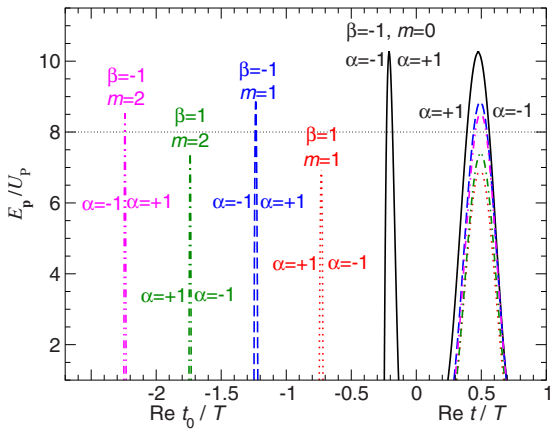

FIG. 1. (Color online) Examples of the notation $\alpha\beta m$ used to label the solutions of the saddle-point equations. The solid, dotted, long-dashed, dot-dashed, and double-dot-dashed curves in the right-hand part of the figure ($0 \leqslant t \leqslant T$) specify the rescattering times for the five pairs of orbits with the shortest travel times. In the left-hand part of the figure, the counterpart of each curve identifies the corresponding ionization times. The emitted electron energy in multiples of U_P is plotted on the ordinate, and horizontal lines (at constant energy) relate ionization times and rescattering times for the respective orbits. There are infinitely many further solutions that have ionization times t_0 beyond the left-hand margin of the figure. Their maximal return energies converge to $8U_\mathrm{P}$. The curves have been calculated for He, for emission in the direction $\theta = 0°$, and for a linearly polarized laser field having the intensity 10^{15} W/cm^2 and the wavelength 760 nm.

In Ref. [36], approximate analytical solutions of the system of saddle-point equations for high-order harmonic generation were found. These solutions were obtained by supposing that the stationary momentum $\mathbf{k}_s$ is small, which is true for long travel times $\mathrm{Re}(t - t_0)$. A similar procedure can be followed for high-order ATI. For this purpose, we consider a linearly polarized laser field with the vector potential $A(t) = A_0 \cos \omega t$ and introduce new variables: $\varphi_0 = \omega t_0$, $\varphi = \omega t$, $q = p/A_0$, and $k = k_s/A_0$. In this notation, the system (15) and (16) reduces to

$$(k + \cos \varphi_0)^2 + \gamma^2 = 0,$$

$$q^2 = 2(k - q \cos \theta) \cos \varphi + k^2, \tag{20}$$

where the scaled stationary momentum is

$$k = (\sin \varphi_0 - \sin \varphi)/(\varphi - \varphi_0) \tag{21}$$

and $\gamma = \sqrt{I_\mathrm{P}/(2U_\mathrm{P})}$ is the Keldysh parameter [60]. The solution of the second equation in Eq. (20) over φ is

$$\varphi = (1 - \alpha)\pi + \alpha \arccos\left(\frac{q^2 - k^2}{2k - 2q \cos \theta} \right), \quad \alpha = \pm 1, \tag{22}$$

which explains the origin of the index α [61]. The solution φ_0 is the same as for high-order harmonic generation

$$\varphi_0 = \beta\left(\frac{\pi}{2} + \frac{k}{\sqrt{1+\gamma^2}}\right) - 2m\pi + i\,\mathrm{arcsinh}\,\gamma, \quad \beta = \pm 1, \tag{23}$$

which shows where the indexes β and m come from: $m=1,2,\ldots$ for $\beta=+1$, and $m=0,1,2,\ldots$ for $\beta=-1$. Letting $k^{(0)}=0$ in Eqs. (22) and (23), we obtain the zeroth-order approximations $\varphi^{(0)}$ and $\varphi_0^{(0)}$. Introducing these solutions into the expression for k, Eq. (21), we obtain the first-order approximation $k^{(1)}$. The first-order approximation for φ_0 and φ is obtained by substituting the $k^{(1)}$ so obtained into the relations $\varphi_0^{(1)}=\varphi_0^{(0)}+\beta k^{(1)}/\sqrt{1+\gamma^2}$ and $\varphi^{(1)}=\varphi^{(0)}+\alpha k^{(1)}/[2\cos^2\theta\sqrt{1-q^2/(4\cos^2\theta)}]$. Using these approximate solutions as the initial solutions, the saddle-point solutions φ_0 and φ can easily be found solving the system of saddle-point equations numerically.

D. Uniform approximation

It is known that the saddle-point method fails for electron energies near and beyond the cutoff [3]. Near their cutoff, the two solutions of one pair approach each other very closely, invalidating the assumption of the SPA that each saddle point can be treated separately. After the cutoff, one solution of each pair is unphysical and does not contribute to the sum (17). This problem has been solved by dropping the unphysical solution for energies higher than the cutoff energy. However, this procedure generates unphysical small spikes around the respective cutoffs. A better and mathematically more rigorous way to solve this problem is to use a uniform approximation for the case of coalescing saddle points [56,62]. This method has already been successfully applied to high-order ATI [35], to high-order harmonic generation [36,58], and to laser-assisted electron-atom scattering [63]. The T-matrix element (17) in the uniform approximation takes the form

$$\begin{aligned} T_{\mathbf{p}i}^{(1)}(n) &= \sum_{\alpha\beta m} A_{\alpha\beta m}\exp(iS_{\alpha\beta m}) \\ &= \sum_{\beta m} (6\pi S_-)^{1/2}\exp(iS_+ + i\pi/4) \\ &\quad \times \left[\frac{A_-}{\sqrt{z}}\mathrm{Ai}(-z) + \frac{iA_+}{z}\mathrm{Ai}'(-z)\right], \end{aligned} \tag{24}$$

where Ai and Ai′ are the Airy function and its first derivative, respectively, and $z=(3S_-/2)^{2/3}$. The quantities $A_\pm$ and $S_\pm$ are related to the weights and the actions of the saddle points in Eq. (17): $A_\pm=(A_{1\beta m}\pm A_{-1\beta m})/2$, $S_\pm=(S_{1\beta m}\pm S_{-1\beta m})/2$. In Eq. (24), beyond the cutoff the argument z must be replaced by $z\exp(i2\beta\pi/3)$, in order to select the proper branch of the Airy functions, and $A_{\alpha\beta m}$ should change its sign.

In Fig. 2 we have compared the results obtained using the uniform approximation with the results obtained using the improved SFA which includes numerical integration over the ionization and travel times. The agreement is excellent. The differences in the low-energy part are due to the dominance of direct ionization for $E_\mathbf{p}<3U_\mathrm{P}$, which is not taken into account in our uniform approximation.

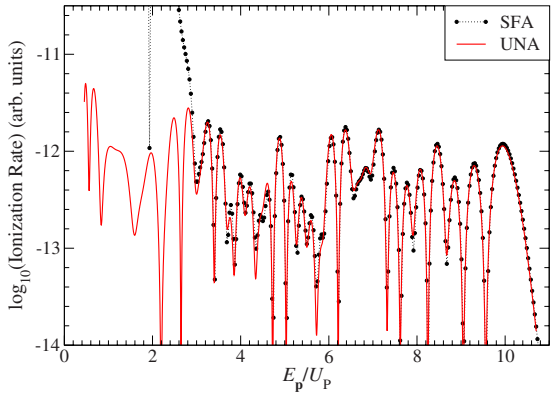

FIG. 2. (Color online) Differential ionization rate of He as a function of the electron kinetic energy $E_\mathbf{p}$ in units of the ponderomotive energy U_P, for emission in the direction $\theta=0°$, for a linearly polarized laser field having the intensity 10^{15} W/cm^2 and the wavelength 760 nm. Comparison of the uniform approximation (UNA) with the results obtained by numerical integration (SFA).

III. SEMICLASSICAL ANALYSIS AND THE CUTOFF LAW

In Ref. [12], using relations (15) and (16), we have derived the semiclassical cutoff law

$$E_{\mathbf{p},\max} = 10.007U_\mathrm{P} + 0.538I_\mathrm{P}. \tag{25}$$

It displays the I_P-dependent correction to the well-known $10U_\mathrm{P}$ classical cutoff law for high-order ATI [10]. The cutoff law (25) is valid for $\theta=0°$ and 180°. For all other values of θ the cutoff value is lower, i.e., the rescattering plateau is shorter. Analogous results for an arbitrary emission angle θ can be obtained solving the system (15) and (16) [11]. In Fig. 3 an example of $(E_\mathbf{p}/U_\mathrm{P})_\mathrm{max}$, obtained in the limit of small Keldysh parameter γ, is presented as a function of the angle θ. The well-known symmetry upon $\theta\leftrightarrow\pi\pm\theta$ [3–5] is clearly visible in Fig. 3.

In Sec. II C we have introduced a classification of the quantum orbits. Each pair of orbits βm is characterized by its own cutoff. It will be useful to analyze how these cutoffs

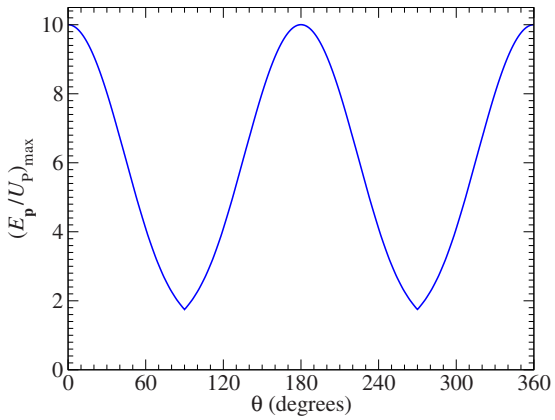

FIG. 3. (Color online) Maximal classical electron kinetic energy as a function of the angle between the emitted electron and the linearly polarized laser field direction.

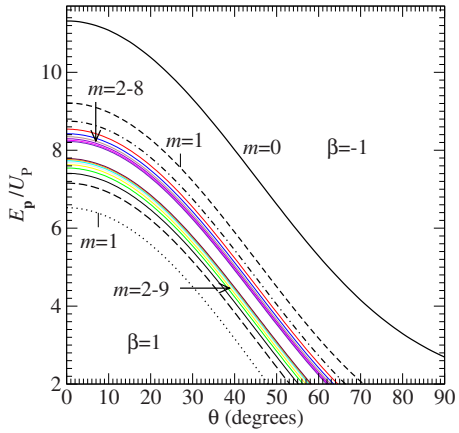

FIG. 4. (Color online) The θ-dependence of the cutoff values for the saddle-point solutions characterized by the index βm (see the text for more explanations).

depend on the angle θ. In Fig. 4, we present the θ-dependence of the cutoff values for various orbits βm, for Xe, and for a linearly polarized laser field having the intensity 8×10^{13} W/cm^2 and the wavelength 760 nm. There are two groups of orbits: orbits with $\beta=-1$ approach, with increasing m a certain θ-dependent limit value from above, while orbits with $\beta=1$ approach the same value from below. For $\theta=0$ the maximum cutoff is for $\beta m=-10$: $(E_{p,\theta=0})_{\max}=11.32U_P$, which is approximately equal to the result obtained using Eq. (25): $10.007U_P+0.538I_P=11.5U_P$. The minimum cutoff is for $\beta m=11$: $(E_{p,\theta=0})_{\max}=6.526U_P$. For both solutions $\beta=-1$ and 1, the value $(E_{p,\theta=0})_{\max}=8U_P$ is approached with increasing m. This is in accordance with the cutoff law for electron-atom scattering: $E_{\mathbf{p}_f}=E_{\mathbf{p}_i}+8U_P\pm4\sqrt{2E_{\mathbf{p}_i}U_P}$, presented in Refs. [64,65], and with the fact that for long orbits (large values of m) the electron initial kinetic energy $E_{\mathbf{p}_i}$ becomes lower and lower. The cutoff values for all solutions βm behave in the same way with increasing θ: the corresponding maximal electron energy slowly decreases toward a value lower than $2U_P$ for $\theta=90°$. Only for the solution with $m=0$ and for not too small values of γ can the minimum cutoff value for $\theta=90°$ be larger than $2U_P$, as shown in Fig. 4. There are no intersections of the cutoff curves.

IV. CONDITION FOR THE CONSTRUCTIVE INTERFERENCE OF THE PARTIAL *T*-MATRIX CONTRIBUTIONS

According to Eq. (17), the T-matrix element is the sum of partial contributions, which correspond to different saddle-point solutions. In order to analyze the interference of these partial contributions, it is convenient to present the rescattering T-matrix element in the form $T^{(1)}_{\mathbf{p}i}(n)=\Sigma_s a_s\exp(i\Phi_s)$, where $a_s>0$ and Φ_s are real. The interference will be constructive if all partial contributions are in phase.

Let us find these phases for the solutions (22) and (23) in the limit of small stationary momenta k, i.e., for long travel times [30]. Taking into account the relations $\sin\varphi_0^{(0)}=\beta\sqrt{1+\gamma^2}$ and $\sin\varphi^{(0)}=\alpha\sin\{\arccos[-q/(2\cos\theta)]\}=\alpha\sqrt{1-q^2/(4\cos^2\theta)}$ to lowest order in $1/(2m\pi)$ we obtain

$$k^{(1)}=\frac{1}{2m\pi}[\beta\sqrt{1+\gamma^2}-\alpha\sqrt{1-q^2/(4\cos^2\theta)}]. \tag{26}$$

Then, using Eq. (18), we find

$$\mathrm{Re}\,S_{\alpha\beta m}=\frac{4U_P}{\omega}\left(\frac{q^2}{2}\varphi^{(0)}+q\cos\theta\sin\varphi^{(0)}\right)+\frac{I_P+U_P}{\omega}\mathrm{Re}\,\varphi_0^{(0)}, \tag{27}$$

where the corrections of the order $1/(2m\pi)$ were neglected (we have also found the higher-order corrections but will not present them here). For $\theta=180°$ this result agrees with that of Ref. [30]. Introducing the solutions $\varphi_0^{(0)}$ and $\varphi^{(0)}$ into Eq. (27), we obtain explicitly

$$\mathrm{Re}\,S_{\alpha\beta m}=\frac{4U_P}{\omega}\left\{\frac{q^2}{2}\left[\pi-\alpha\arccos\left(\frac{q}{2\cos\theta}\right)\right]+\alpha q\cos\theta\sqrt{1-\frac{q^2}{4\cos^2\theta}}\right\}+\frac{I_P+U_P}{\omega}\left(\beta\frac{\pi}{2}-2m\pi\right). \tag{28}$$

Further contributions to the phase Φ_s come from the matrix elements in Eq. (17) and from Δ_s, Eq. (19). Keeping only the zeroth order terms in $1/(2m\pi)$, it can be shown that Δ_s has the opposite sign for $\alpha=1$ and -1, so that

$$\Delta_s^{-1/2}\propto\exp[i(\alpha-1)\pi/4]. \tag{29}$$

It can also be shown that $V_{\mathbf{k}_s-\mathbf{p}}=V_{-\mathbf{p}}$ plus corrections of the order $1/(2m\pi)$, so that this matrix element does not contribute to the phase Φ_s. Let us now analyze the matrix element $M_{0s}=\langle\mathbf{k}_s+\mathbf{A}(t_{0s})|\mathbf{r}\cdot\mathbf{E}(t_{0s})|\psi_i\rangle$, which appears in Eq. (17), for the initial Hartree-Fock wave functions [11]. This matrix element can be calculated analytically, but we will not present here these cumbersome expressions. If, in these expressions, we take into account that $[\mathbf{k}_s+\mathbf{A}(t_0)]^2=-2I_P$, Eq. (15), then, for our linearly polarized laser field, we obtain

$$M_0\propto\begin{cases}\sin\varphi_0(k+\cos\varphi_0) & \text{(for an } s \text{ ground state)}\\ \sin\varphi_0 & \text{(for a } p \text{ ground state)}\end{cases}. \tag{30}$$

Taking into account that $\sin\varphi_0^{(0)}=\beta\sqrt{1+\gamma^2}$ and $k^{(1)}+\cos\varphi_0^{(1)}=-i\beta\gamma$, we get

$$M_0\propto\exp[i(1-\beta)l\pi/2], \tag{31}$$

where $l=0$ for s states and $l=1$ for p states. Taking also into account relations (28) and (29), we finally have

$$\Phi_{\alpha\beta m}=\mathrm{Re}\,S_{\alpha\beta m}+(\alpha-1)\pi/4+(1-\beta)l\pi/2. \tag{32}$$

With the abbreviation

$$I_P+U_P\equiv n_c\omega, \tag{33}$$

from relations (28) and (32) it follows that

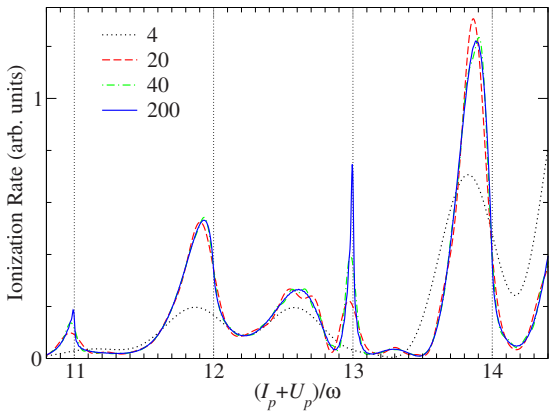

FIG. 5. (Color online) Differential ionization rate of Kr as a function of the parameter $(I_P+U_P)/\omega$, for emission of electrons with kinetic energy $E_p=23$ eV in the direction $\theta=0°$. The laser field is linearly polarized having the wavelength 760 nm. Its intensity changes from 0.67×10^{14} to 1.76×10^{14} W/cm^2. The uniform approximation for high-order ATI is used with 4 (black dotted curve), 20 (red long-dashed curve), 40 (green dot-dashed curve), and 200 (blue solid curve) quantum orbits.

$$\Phi_{\alpha 1m} - \Phi_{\alpha -1m} = (n_c - l)\pi. \tag{34}$$

In Refs. [30,36], only the case $l=0$ was considered and it was found that the interferences are constructive for even n_c. Then, from relation (34) it follows that the constructive interferences and the resonantlike enhancements for p states ($l=1$) should be obtained for odd n_c in Eq. (33).

V. ANALYSIS OF HIGH-ORDER ATI ENHANCEMENTS IN TERMS OF LONG QUANTUM ORBITS

It is known that a small number of quantum orbits is sufficient to approximately calculate the high-order ATI spectra within the saddle-point approximation [3]. Figure 4 shows that in the cutoff region only the two orbits with $\beta m=-10$ contribute. We have also shown, in Sec. II D, that the appearance of artificial spikes in the high-order ATI spectrum near the cutoffs of particular pairs of orbits $1\beta m$ and $-1\beta m$ (see, for example, Fig. 4 in Ref. [11]) is avoided by using the uniform approximation. In the middle part of the spectrum, i.e., in the plateau region, more orbits have to be taken into account. Due to wave-packet spreading, the amplitudes of the partial T-matrix elements decrease with increasing length of the orbits. Since, in most cases, their phases are random, the convergence of the sum (24) can be achieved with a small number of orbits. However, near a channel closing the phases of the long orbits add constructively so that very many orbits have to be taken into account.

We illustrate this with an example of ATI spectra of Kr atoms, presented in Fig. 5. The laser field is linearly polarized having the wavelength of 760 nm and its intensity changes from 0.67×10^{14} to 1.76×10^{14} W/cm^2, so that the parameter $(I_P+U_P)/\omega$ takes on values between 10.8 and 14.4 and encompasses four CCs: $n_c=11$, 12, 13, and 14 [see Eq. (33)]. It is obvious that four orbits (the black dotted curve in Fig. 5) only produce a very rough approximation to the exact yield. However, including 200 orbits does not significantly change the sum of 20 orbits, except near CCs, where the former exhibits extremely sharp spikes exactly at the odd CCs $n_c=11$ and 13. According to Refs. [46–48], the enhancements are threshold phenomena, which appear at even CCs for even l and at odd CCs for odd l (as is the case in our example for the p ground state of Kr). Our analysis suggests that the enhancements are due to the constructive interference of the contributions of the long orbits. The constructive interference of about the first 20 orbits leads to the appearance of enhancements in the region 5%–10% below even CCs. These enhancements we will call type-I enhancements. Long orbits imply a long travel time, i.e., these orbits can only develop if the pulse duration is long enough. Still longer orbits (e.g., orbits 50–100 and longer) give rise to the very sharp enhancements that are located precisely at the odd CCs. We will refer to the latter as type-II enhancements.

In order better to understand the behavior of the spectra shown in Fig. 5, we will analyze the relative phase $\Delta\Phi(m)=\Phi_{\beta=-1}-\Phi_{\beta=+1}$ of the partial contributions to the T-matrix element (24) for fixed values of m. If $\Delta\Phi(m)=(2k+1)\pi$ with integer k, the contributions with $\beta=1$ and $\beta=-1$ for ionization within the mth past period are out of phase. If this is so for all $m>m_0$ with $m_0\gg1$, a constructive interference of the contributions of the long orbits cannot develop. If, on the other hand, $\Delta\Phi(m)=2k\pi$ with integer k for $m>m_0$, constructive interference is likely. Figure 6 shows that the latter condition is satisfied for $n_c=11$ with $m_0=0$. Indeed, Fig. 5 exhibits a pronounced spike at $n_c=11$. In contrast, for $n_c=12$ we infer from Fig. 6 that the orbits with $m>m_0=5$ will all interfere destructively, in agreement with the observation from Fig. 5 that 20 orbits suffice to approximate the exact result near $n_c=12$ and that the resulting yield forms a smooth maximum. These patterns repeat themselves near $n_c=13$ and 14. A very interesting observation from Fig. 6(b) is that just below $n_c=12$ for $m\geqslant6$ the phase differences jump up by π to settle near a value close to zero for a short n_c interval. Indeed, this is approximately where Fig. 5 displays the type-I enhancement.

Let us now analyze an example of the He atom, whose ground state has even parity ($l=0$). Since the ionization energy and the saturation intensity of He are larger than for Kr, the final electron kinetic energy E_p can also be larger. In Fig. 7 we present the ionization rate of He for $E_p=199$ eV. The laser field is linearly polarized having the wavelength 760 nm and its intensity changes from 1.04×10^{15} to 1.16×10^{15} W/cm^2, so that the parameter $(I_P+U_P)/\omega$ assumes values between 49.5 and 53.4 and encompasses four CCs: $n_c=50$, 51, 52, and 53. As in the Kr case, the spectrum cannot be well described with only four orbits; but the results for 20 and 200 orbits agree well most of the time so that 20 orbits are sufficient. The exception is the immediate vicinity of the CCs, where 200 (or possibly more; cf. Fig. 11) orbits are needed. These enhancements are particularly sharp for even n_c. They are so sharp that they are just barely visible in Fig. 7; see Fig. 12 below for an enlargement. Each of these spikes is preceded by a pronounced peak. These peaks can be approximated well with 40 orbits but not with 20 orbits. For even CCs these peaks are closer to n_c and can easily be

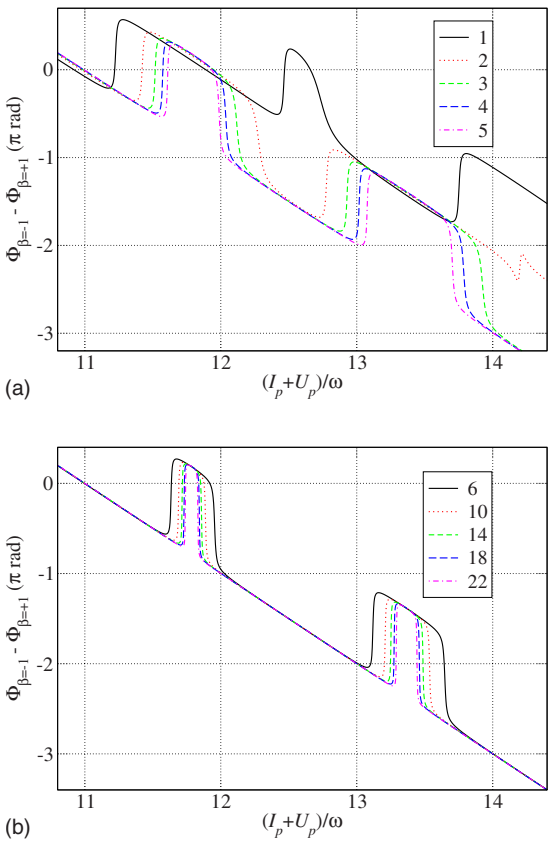

FIG. 6. (Color online) The relative phase $\Phi_{\beta=-1}-\Phi_{\beta=+1}$ of the mth partial contribution to the T-matrix element in the uniform approximation (24) as a function of the parameter $(I_P+U_P)/\omega$, for the atomic and laser field parameters of Fig. 5. The results presented are (a) for $1 \leqslant m \leqslant 5$ and (b) for $6 \leqslant m \leqslant 22$ in steps of 4.

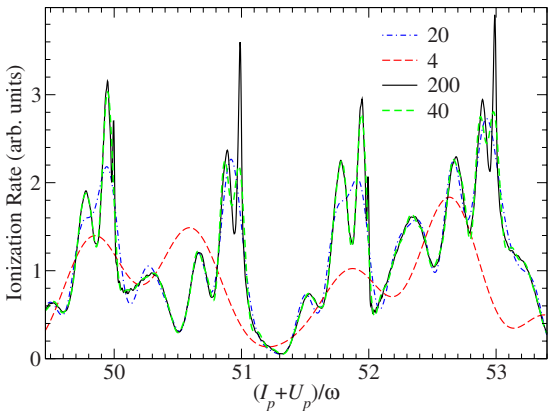

FIG. 7. (Color online) Differential ionization rate of He as a function of the parameter $(I_P+U_P)/\omega$, for emission of electrons with kinetic energy $E_{\mathbf{p}}=199$ eV in the direction $\theta=0°$. The laser field is linearly polarized having the wavelength 760 nm. Its intensity changes from 1.04×10^{15} to 1.16×10^{15} W/cm^2. The uniform approximation for high-order ATI is used with 4 (red dashed curve), 20 (blue dot-dashed curve), 40 (green long dashed curve), and 200 (black solid curve) quantum orbits.

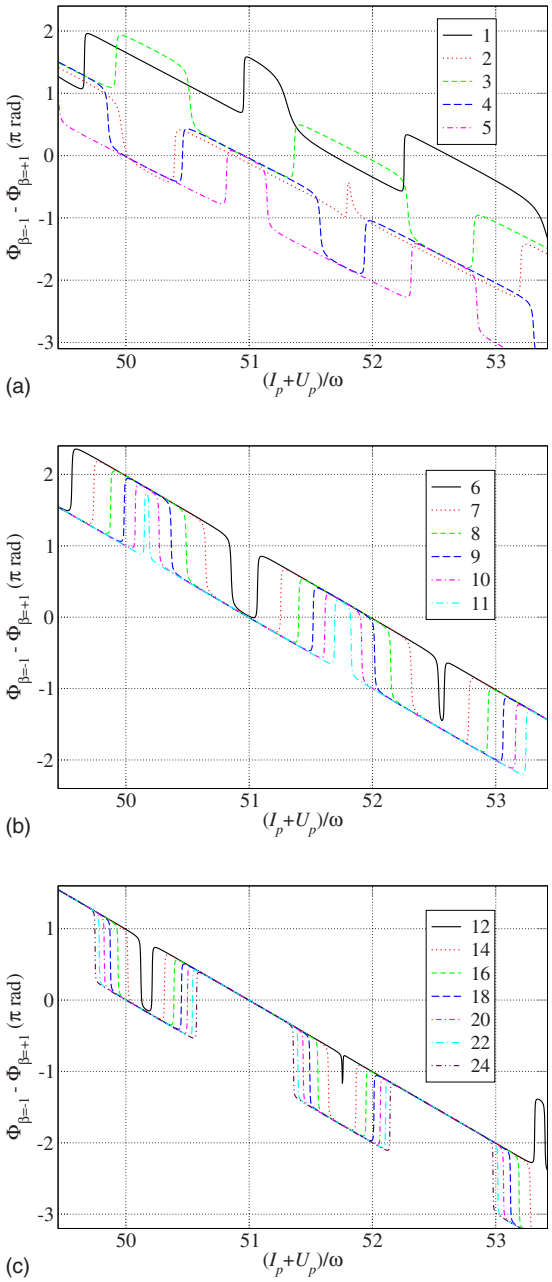

FIG. 8. (Color online) The relative phase $\Phi_{\beta=-1}-\Phi_{\beta=+1}$ of the mth partial contribution to the T-matrix element in the uniform approximation (24) as a function of the parameter $(I_P+U_P)/\omega$, for the atomic and laser field parameters of Fig. 7. The results presented are (a) for $1 \leqslant m \leqslant 5$, (b) $6 \leqslant m \leqslant 11$, and (c) for even $12 \leqslant m \leqslant 24$.

misinterpreted as the spiky type-II enhancements, which appear exactly at CCs. For the s ground state of He, we expect to have the type-II enhancements for even CCs. However, we see that they appear also for odd CCs.

To summarize the present case of He, we observe both types of enhancements at each CC, regardless of whether n_c is even or odd. The constructive interference of 30–40 orbits leads to the appearance of type-I enhancements in the region 5%–10% below each CC. Very long orbits (orbits 50–400) give rise to the extremely sharp type-II enhancements, which are located precisely at the CCs. The qualitative difference

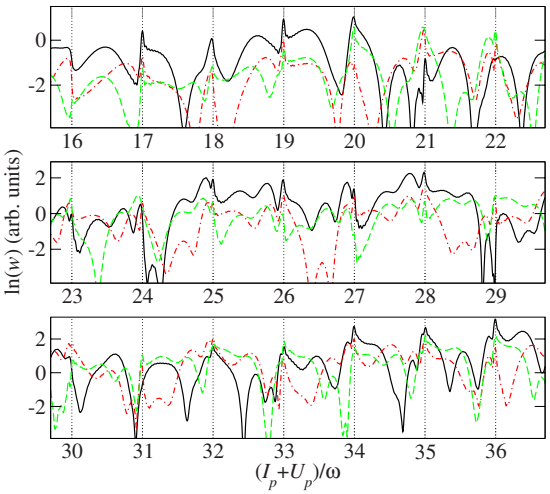

FIG. 9. (Color online) Natural logarithm of the differential ionization rate of Xe as a function of the parameter $(I_P+U_P)/\omega$, for emission of the electrons having kinetic energy $E_p=90$ eV in the direction $\theta=0°$. The laser field is linearly polarized having the wavelength 760 nm. Its intensity changes from 2.5×10^{14} to 8×10^{14} W/cm^2. The uniform approximation for high-order ATI is used with 100 quantum orbits (black solid curve). The results with only the orbits having $\beta=1$ ($\beta=-1$) included are presented by the red dot-dashed (green long dashed) curve.

between the results for Kr, presented in Fig. 5, and the results for He (Fig. 7) is apparently due to different electron kinetic energy and laser intensity regions.

As in the previous case of Fig. 5, further insight can be gained by inspection of the phase differences $\Delta\Phi(m)$. We exhibit the latter in Fig. 8 and invite the reader to study the very complex relation between the phases and the yields. As one example, Fig. 8(c) shows that only the orbits with $m>14$ conspire to build up the very narrow type-II spike at $n_c=50$.

As a final example, we analyze the high-order ATI spectra of Xe atoms for which the enhancements are expected for odd n_c, since $l=1$ for the ground state of Xe. In Fig. 9 we show the yield of 90-eV electrons emitted in the laser polarization direction for n_c between 16 and 36. We see that the enhancements appear both for even and odd n_c and that for some values of n_c there are no enhancements at all. In order to explain these results we have also presented the partial rates, obtained using the uniform approximation (24), for fixed values of the subindex β, summed over all values of m. Recall from Figs. 1 and 4 that orbits with $\beta=1$ have a cutoff below the very-long-orbit cutoff limit $(m\to\infty)$ and those with $\beta=-1$ above. The energy of 90 eV is well below $8U_P$ even at the lowest intensity considered so that orbits with $\beta=1$ and with $\beta=-1$ on the average will contribute equally. For $16\leqslant n_c\leqslant 20$ the amplitudes of the contributions from $\beta=1$ (red dot-dashed curve) and from $\beta=-1$ (green long dashed curve) interfere constructively leading to sharp peaks in the differential rate summed over m (black solid curve). However, with a further increase of n_c up to $n_c=24$, the interference is destructive and the peaks are less pronounced or completely disappear. The interference is again constructive for n_c from 25 to 28. This is followed by subsequent intervals of destructive and constructive interferences. For Xe, Eq. (34), viz. $\Phi_{\alpha 1m}-\Phi_{\alpha-1m}=(n_c-l)\pi$ with $l=1$, seems to favor enhancements for odd n_c. We observe from Fig. 9 that this prediction is not reliable. It is more appropriate for lower electron energies and laser intensities, as in Fig. 5.

VI. THRESHOLD ANOMALIES IN HIGH-ORDER ATI

Threshold anomalies are a well-known phenomenon in the theory of collisions and reactions [38–43]. If a cross section is considered as a function of energy, these anomalies manifest themselves in the form of "Wigner cusps" (upward or downward) and "steps" [rounded upward (S-like) or downward step] at the threshold energies. We will now show that these features also occur for ATI, even though this is induced by a time-dependent external field.

Our intensity-dependent enhancements occur in the plateau region of the electron energy spectra. Since the rescattering ATI amplitude is responsible for this part of the spectrum, in the Appendix we derived the expression (A7) for the corresponding rescattering T-matrix element for ATI with absorption of n laser photons:

$$T_{\mathbf{p}i}^{(1)}(n)=\sum_{n'}\int d^3\mathbf{k}T_{\mathbf{pk}i}(n,n')\int_0^\infty d\tau e^{-i[E_{\mathbf{k}}+(n_c-n')\omega]\tau}, \tag{35}$$

with $T_{\mathbf{pk}i}(n,n')=-iT_{\mathbf{pk}}^{(0)}(n-n')T_{\mathbf{k}i}^{(0)}(n')$ and $n_c\omega=I_P+U_P$. This result is in accordance with the three-step model of high-order ATI: direct ionization with absorption of n' laser photons is followed by propagation of the electron with momentum $\mathbf{k}$ in the laser field during the time τ and subsequent laser-assisted potential scattering in which $n-n'$ photons are exchanged with the laser field. The expression (35) also includes the integration over all travel times τ and over all intermediate electron momenta $\mathbf{k}$, as well as the summation over all integer values of n'.

The threshold anomalies of time-independent scattering theory are connected with the nonanalyticity of the transition amplitude at the threshold energy. The corresponding momenta are small. In our case an electron "born" with drift momentum near zero can acquire a much higher drift momentum during the subsequent steps. This is exactly what happens in high-order ATI: the small quantity is the drift momentum $\mathbf{k}_s$ of the electron in the intermediate state (between ionization and rescattering); see Sec. II. The ionization happens at the threshold $k_s=0$ and the subsequent laser-assisted electron scattering cannot "delete" the anomalies introduced by this ionization threshold. Furthermore, since $k_s\propto 1/(t-t_0)$, small k_s implies long travel time and long orbits, which is in agreement with the fact that at the threshold a large number of saddle-point solutions has to be taken into account.

In the Appendix, we have obtained the expressions (A8) and (A9) for the expansion of the rescattering T-matrix in the small intermediate electron momentum $\mathbf{k}$. This can be rewritten as

$$T_{\mathbf{p}i}^{(1)}(n) \approx R_{\mathbf{p}i}(n) + A_{\mathbf{p}i}(n,n_c')\sqrt{n_c' - n_c}, \tag{36}$$

where we have explicitly separated the term $n' = n_c'$, with n_c' the integer nearest n_c, from the remaining part $R_{\mathbf{p}i}(n)$ of the sum over n'. According to Eq. (A9) it is $A_{\mathbf{p}i}(n,n_c') = i(2\pi)^2\sqrt{2\omega}T_{\mathbf{p}\mathbf{0}}^{(0)}(n-n_c')T_{\mathbf{0}i}^{(0)}(n_c')$, while, in general, it may be proportional to an integer power of $n_c' - n_c$. Denoting $R_{\mathbf{p}i}A_{\mathbf{p}i}^* = a\exp(i\varphi)$ with real positive a and the real phase φ, we obtain

$$|T_{\mathbf{p}i}(n)|^2 = |R_{\mathbf{p}i}(n)|^2 + |A_{\mathbf{p}i}(n,n_c')|^2|n_c' - n_c| + 2a\sqrt{|n_c' - n_c|} \times \begin{cases} \cos\varphi, & n_c' > n_c \\ \sin\varphi, & n_c' < n_c \end{cases}. \tag{37}$$

Therefore if we consider the rescattering T-matrix element as an analytical function of the parameter n_c, we see that the nonanalyticity (and the threshold anomaly) appears at $n_c = n_c'$. The above expression shows that, as a function of n_c (that is, as a function of intensity), around the n_c'th channel closing the derivative of $|T_{\mathbf{p}i}(n)|^2$ with respect to n_c is infinite ($\propto|n_c' - n_c|^{-1/2}$) and $|T_{\mathbf{p}i}(n)|^2$ exhibits an upward (downward) cusp for φ in the first (third) quadrant, and a rounded upward (downward) step for φ in the second (fourth) quadrant.

The appearance of all four types of threshold anomalies is not always possible. For example, for scattering cross sections in the case when below the considered threshold there is only one open channel, the S-like step and downward cusp are not possible [42,66]. In this case, immediately above threshold the cross section cannot increase. Our results, presented in Figs. 5, 7, and 9, exhibit only upward cusps and downward steps, though in some cases this is hard to tell.

It should be mentioned that the threshold anomalies are modified in the presence of the Coulomb interaction [67,68]. In our theory, the long-range Coulomb interaction is neglected and we will not discuss this here.

After we have realized that the threshold anomalies should appear for high-order ATI, let us now, again using the results of the Appendix, investigate analytically the connection of the type of the ground state (s or p) and the parity of n_c. In the term $A_{\mathbf{p}i}$ in Eq. (36) the T-matrix element $T_{\mathbf{p}\mathbf{0}}^{(0)}(n-n')$ is real, while $T_{\mathbf{0}i}^{(0)}(n')$ is expressed as the Fourier transform of Eq. (A6). The matrix element in Eq. (A6) can be calculated analytically. This matrix element is multiplied by the exponential function $\exp[i\mathcal{U}_1(t_0)] = \exp[ia\sin(2\omega t_0)]$, with $a = U_P/(2\omega)$, which can be expanded in Bessel functions as $\Sigma_m J_m(a)\exp(2im\omega t_0)$. Since we have $2m$ in the exponent it can be shown that for s states $T_{\mathbf{0}i}^{(0)}(n') = 0$ for odd n', while for p states $T_{\mathbf{0}i}^{(0)}(n') = 0$ for even n'. Therefore the enhancements for the s states (p states) occur for even (odd) n_c. This is in agreement with previous results. These dominant enhancements correspond to long travel times, i.e., long orbits, for which the higher-order terms in the expansion (A8) can be neglected (the wave-packet spreading term is $\propto\tau^{-3/2-s}$, $s = 0,1,2,\ldots$). There are also less pronounced enhancements which can appear both for even and odd n_c and correspond to not so long orbits. Namely, for the higher-order terms the expansion of $\exp[i\mathbf{k}\cdot\boldsymbol{\alpha}(t_0) + i\mathcal{U}_1(t_0)]$ in terms of the generalized Bessel functions gives the factor $\exp(im\omega t_0)$ so that the enhancements may be encountered both for even and for odd n_c. Furthermore, the second term in the last row of Eq. (A8) is proportional to $(n' - n_c)^{3/2}$ so that the type of the enhancement can change.

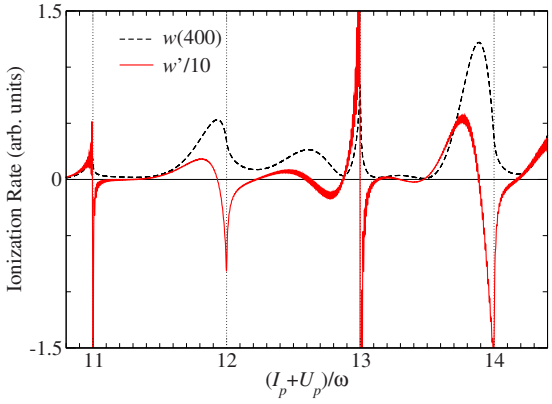

FIG. 10. (Color online) The same as in Fig. 5 but for 400 orbits. The derivative of the ionization rate (divided by the factor 10) over the parameter $n_c = (I_P + U_P)/\omega$ as a function of n_c is also presented by a red solid line.

In order to illustrate how the threshold anomalies are related to our type-I and type-II enhancements, in Fig. 10 we present the ionization rate and its derivative over the parameter $n_c = (I_P + U_P)/\omega$ as functions of n_c for the same laser and atomic parameters as in Fig. 5, calculated using the uniform approximation with 400 orbits. For odd n_c, it is obvious that the type-II enhancements are upward cusps. Very close to $n_c = 11$ and 13, the first derivative w' goes from $+\infty$ to $-\infty$, which is in agreement with the derivative of Eq. (37). From the previous analysis, the nature of the type-I enhancements was not quite clear. Now, from Fig. 10 it follows that for $n_c = 12$ and 14 the first derivative of the rate over n_c goes to $-\infty$. This corresponds to the threshold anomaly called the rounded downward step. For this type of the threshold anomaly the ionization rate, as a function of n_c, has a maximum below the corresponding channel closing.

Another point that should be discussed is the appearance of more than one enhancement near the same value of n_c, as it was illustrated in Fig. 7. In Fig. 11 we present results analogous to Fig. 7 but for 400 orbits and with the first derivative of the ionization rate also shown. At each of the four channel closings covered by the figure, we observe an upward cusp (those at $n_c = 50$ and 52 are just barely visible). On top of that and dwarfing the cusps at $n_c = 50$ and 52, we notice two different rounded-downward-step threshold anomalies. In order to illustrate this more precisely, in Fig. 12 we present an enlarged part of Fig. 11 around $n_c = 50$. The presence of the upward cusp at $n_c = 50$ is revealed by the fact that the derivative w' of the ionization rate goes from $+\infty$ just below $n_c = 50$ to $-\infty$ just above $n_c = 50$. The additional two rounded downward steps are connected with the rate maxima at $n_c = 49.78$ and 49.95. At these values of n_c, the derivatives of the respective terms in the ionization rate each start to decrease to $-\infty$, which they reach at $n_c = 50$, but, since the upward-cusp-threshold anomaly takes over, these rounded-downward-step threshold anomalies manifest themselves as

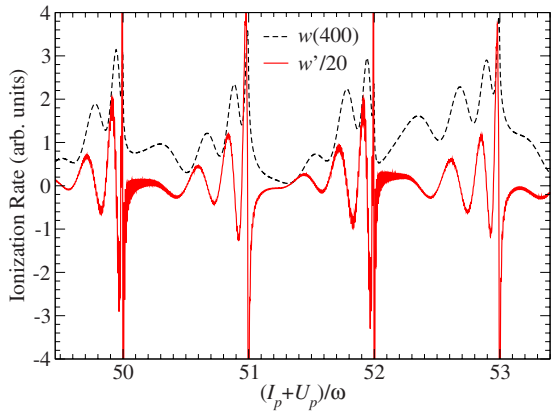

FIG. 11. (Color online) The same as Fig. 7 but for 400 orbits. The derivative of the ionization rate (divided by the factor 20) over the parameter $n_c=(I_P+U_P)/\omega$ as a function of n_c is also presented by the red solid line.

minima in the derivative of the rate. Therefore we have an interplay of several different threshold anomalies. At a particular channel closing one type of threshold anomaly is dominant but, depending on the laser field and atomic parameters and on the electron energy, the contributions of other anomalies, which are related to higher order terms in Eq. (A8), may become important.

VII. NUMERICAL EXAMPLES

In this section, we present energy spectra for Xe atoms, obtained using the improved SFA method described in Ref. [11]. We consider only high-order ATI and rescattered electrons emitted in the direction $\theta=0°$. The laser field is linearly polarized having the wavelength 760 nm. In order to see the influence of the parity of the ground state, we model the ground state wave function by a p state as in [11] (these results are presented in Fig. 13) and by a 1s state (Fig. 14). The rescattering potential is the same in both cases and is modeled as in Refs. [11,65].

Let us first analyze Fig. 13, where the logarithm of the differential ionization rate is presented in false colors as a

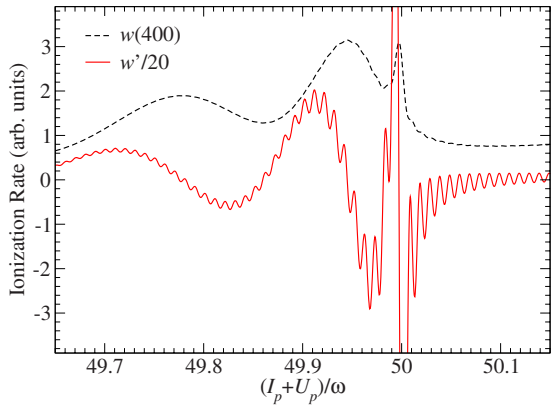

FIG. 12. (Color online) Enlarged part of Fig. 11 near $n_c=50$.

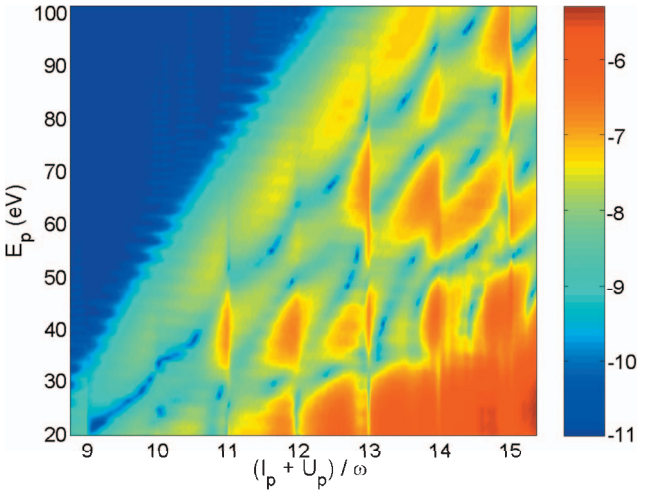

FIG. 13. (Color) High-order ATI photoelectron energy spectrum of Xe ($I_P=12.13$ eV, p ground state [11]), presented in false colors, as a function of the laser intensity expressed in units $(I_P+U_P)/\omega$. Electron emission is in the direction $\theta=0°$, the laser field is linearly polarized having the wavelength 760 nm, and the laser intensity changes from 4×10^{13} to 2.4×10^{14} W/cm^2. Only the rescattering contribution to the T matrix is taken into account, with the rescattering potential modeled as in [11].

function of the electron energy $E_\mathbf{p}$ (in eV) and of the laser intensity, expressed through the parameter $(I_P+U_P)/\omega$ so that integer numbers on the abscissa correspond to the CC numbers n_c. The cutoff region is clearly visible: it extends from 30 eV at $n_c=9$ to 100 eV at $n_c=13$. The enhancements at integer values of n_c are very pronounced. In the region 35–45 eV there are sharp enhancements for $n_c=11$ and 13, while the enhancements for $n_c=12$ and 14 are broader. The next enhancements are for the energies between 60 and 70 eV, where sharp enhancements are for $n_c=13$ and 15, while a broad enhancement is for $n_c=14$. For energies above 80 eV a sharp enhancement appears for $n_c=15$, etc. There are two types of sharp enhancements. One looks like a cusp ($n_c=11$ and $E_\mathbf{p}\approx40$ eV, $n_c=13$ and $E_\mathbf{p}\approx65$ eV, and $n_c=15$

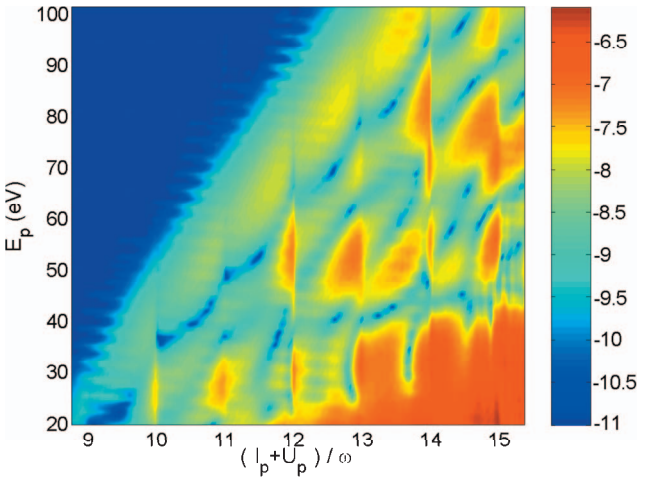

FIG. 14. (Color) Same as in Fig. 13, but for the Xe atom modeled by a 1s ground state. The ionization energy is $I_P=12.13$ eV.

and $E_{\mathbf{p}} \approx 90$ eV), while the other exhibits a broad maximum followed by a minimum ($n_c=13$ and $E_{\mathbf{p}} \approx 40$ eV, and $n_c=15$ and $E_{\mathbf{p}} \approx 65$ eV). For even n_c it seems that the enhancement regions at $n_c=12$ with $E_{\mathbf{p}} \approx 40$ eV and at $n_c=14$ with $E_{\mathbf{p}} \approx 65$ eV are broader than the one at $n_c=14$ with $E_{\mathbf{p}} \approx 40$ eV. All these numerical results are examples of the two types of enhancements described in Sec. V and presented in Fig. 5. For instance, for $E_{\mathbf{p}} \approx 40$ eV the sharp peak at $n_c=11$ is a cusp, which above we classified as a type-II enhancement. The broad peak below $n_c=12$ is a type-I enhancement. Near $n_c=13$ both types appear. The broad peak below $n_c=13$ is the type-I enhancement, while the sharp peak exactly at $n_c=13$ is the type-II enhancement. Finally, the broad peak below $n_c=14$ is a type-I enhancement.

The same results as in Fig. 13, but for the Xe atom modeled by a 1*s* ground state, are shown in Fig. 14. Comparing Figs. 13 and 14, we notice that they are qualitatively very similar except that the role of even and odd CCs is interchanged. For example, the shape and the structure of the enhancements near 40 eV in Fig. 13 at $n_c=11$, 12, 13, and 14, are completely repeated in Fig. 14, but now for energies near 50 eV and for $n_c=12$, 13, 14, and 15. Therefore for the *s* ground state ($l=0$) sharp enhancements appear for even n_c, while for the *p* ground state ($l=1$) they appear for odd n_c. This is in agreement with the saddle-point analysis presented in Sec. IV [see Eq. (34)].

VIII. FOCAL AVERAGING AND THE POSSIBILITY OF OBSERVING TYPE-I AND TYPE-II ENHANCEMENTS

For a simulation of ATI experiments, the energy spectrum of the ionized electrons has to be integrated over the spatiotemporal intensity distribution in the laser focus. The details of our focal-averaging method are described in [29,55] and numerous examples, related to the channel-closing effect, are presented in Ref. [11]. In the focal-averaged spectrum, the effects of channel closings are visible regardless of the value of the peak intensity since the focal volume always contains regions where the laser intensity is close to the channel-closing intensity. Therefore the type-II enhancements always appear in the focal-averaged spectra and manifest themselves as sharp peaks in the spectra at electron energies $E_{\mathbf{p}}=(n-n_{c,\min})\omega$, $n \geqslant n_{c,\min}=[I_P/\omega]+1$. For electrons emitted in the direction $\theta=0$ or $\theta=\pi$, the sharp enhancements are by far most pronounced for electron energies within the interval $5U_P < E_{\mathbf{p}} < 8U_P$ (for details see [11]).

In this section, we will consider the question of whether the type-I enhancements survive the focal averaging, i.e., whether they can be distinguished in an experiment. We calculate the focal-averaged electron spectra of Kr for four different peak intensities: 0.75, 1.06, 1.37, and 1.68×10^{14} W/cm^2, which, in accordance with Fig. 5, are slightly above the channel-closing intensities for the channels $n_c=11$, 12, 13, and 14, respectively. The corresponding focal-averaged electron spectra are presented in Fig. 15. The sharp peaks at the electron energies equal to $n\omega$ correspond to the type-II enhancements for $n_c=11$ and 13 in Fig. 5. They appear in the region $5-8U_{Pc}$ which is 20–32 and 36–58 eV for

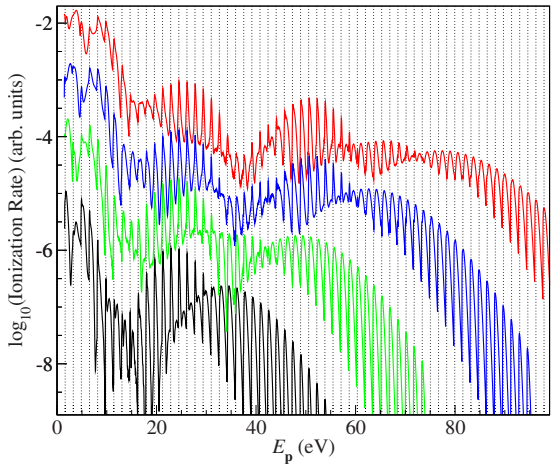

FIG. 15. (Color online) Logarithm of the focal-averaged differential ionization rates of Kr as functions of the electron kinetic energy for emission in the direction $\theta=0°$. The laser field is linearly polarized having the wavelength 760 nm. Its intensity is $a \times 10^{14}$ W/cm^2, where $a=0.75$ (bottom black curve), 1.06 (green curve), 1.37 (blue curve), and 1.68 (upper red curve). The results are obtained using the improved SFA [11] and each upper curve is shifted up by 0.5 units with respect to the lower one.

$n_c=11$ and 13, respectively. In order to investigate the type-I enhancements, in Fig. 16 we present an enlarged part of Fig. 15 for the intensities 1.06 and 1.68×10^{14} W/cm^2 that corresponds to $n_c=12$ and 14, respectively. For $n_c=12$ the interval $5-8U_{Pc}$ [11] corresponds to the electron energies 28–45 eV. In this case, the bottom curve in Fig. 16 exhibits peaks that are not positioned at $E_{\mathbf{p}}=n\omega$ and whose relative distance is not equal to ω. These peaks are less pronounced than the sharp peaks at $E_{\mathbf{p}}=n\omega$. They are related to the type-I enhancements.

Let us explain the position of these peaks. For a fixed laser intensity I corresponding to the ponderomotive energy $U_P=I/(4\omega^2)$, the electron energy is given by the energy-conserving condition $E_{\mathbf{p}}=n\omega-I_P-U_P$. According to Fig. 5,

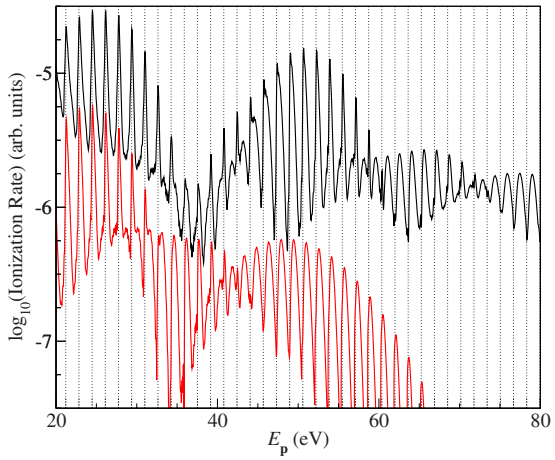

FIG. 16. (Color online) Same as Fig. 15, but for the intensities 1.06×10^{14} W/cm^2 (lower red curve) and 1.68×10^{14} W/cm^2 (upper black curve).

for $E_{\mathbf{p}}=23$ eV, the ionization rate has broad maxima at $I_P+U_P=n_c\omega-\Delta_c$ just below $n_c=12$ and 14. The shift $\Delta_c(E_{\mathbf{p}})$ depends both on the electron energy $E_{\mathbf{p}}$ and on the channel-closing number n_c. Introducing this into the energy-conserving condition we obtain $E_{\mathbf{p}}=(n-n_c)\omega+\Delta_c(E_{\mathbf{p}})$ for the corresponding electron energies. For $n_c=12$ we have used our quantum-orbit theory to calculate that the shift $\Delta_c(E_{\mathbf{p}})$ decreases with increasing electron energy. This is exactly what we observe in the bottom curve in Fig. 16. Furthermore, there are traces of these peaks in the upper curve in Fig. 16 in the region 30–35 eV, where the sharp peaks at $E_{\mathbf{p}}=n\omega$ are dominant.

For $n_c=14$, the interval $5-8U_{Pc}$ corresponds to 44–70 eV. Again, the upper curve in Fig. 16 shows peaks in this region that are not exactly at $n\omega$. Below 60 eV they are mixed with the $n_c=13$ sharp peaks. We conclude that, even though they are not so strong as the sharp type-II enhancements, the type-I enhancements can be distinguished in the experiment. They are characterized by peaks which are shifted with respect to $E_{\mathbf{p}}=n\omega$ and whose relative distance is smaller than ω.

IX. DISAPPEARANCE OF THE ENHANCEMENTS FOR ULTRASHORT LASER PULSES

In this section we will show that the enhancements in high-order ATI spectra disappear for laser pulses which are so short that long orbits do not have enough time to develop. The improved SFA [11] can be generalized to ATI by few-cycle pulses [5]. Without going into the details of this method, we here present numerical results for the focal-averaged ATI spectra of Xe atoms ionized by a linearly polarized few-cycle pulse having the wavelength 760 nm and the intensity 1.1×10^{14} W/cm^2. The pulse envelope is sine square and we consider pulse durations (full width at half maximum of the intensity) of 5.5 fs ($n_p=6$ optical cycles, according to Sec. 4.3 of Ref. [5]), 12.9 fs ($n_p=14$), and 20.3 fs ($n_p=22$). According to the results presented in Table II in Ref. [11], the enhancements due to the $n_c=11$ channel closing appear for energies between 29 and 47 eV. This is clearly visible from the bottom curve in Fig. 17, which corresponds to an infinitely long pulse with a flat envelope. These enhancements become less pronounced for shorter pulses and completely disappear for a few-cycle pulse; see the upper curve, which corresponds to the pulse duration 5.5 fs. These results are in agreement with the experiments [17,18].

X. CONCLUSIONS

The intensity-dependent enhancements in high-order ATI spectra are a fascinating quantum-mechanical phenomenon wanting further analysis and physical interpretation. Our paper gives insights into this problem. With the formalism developed we were able to analyze these enhancements in terms of partial contributions of different quantum orbits to high-order ATI spectra.

We have shown both analytically [see Eq. (34)] and numerically (see Figs. 13 and 14) that the enhanced structures

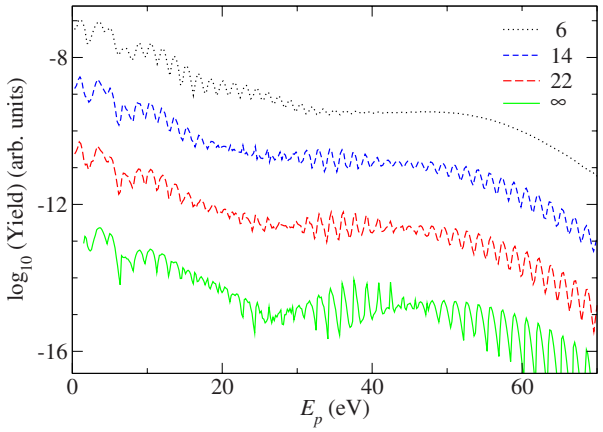

FIG. 17. (Color online) The logarithm of the focal-averaged yield of Xe as a function of the energy of a photoelectron emitted in the polarization direction. The laser field is linearly polarized having the wavelength 760 nm and the intensity 1.1×10^{14} W/cm^2. The bottom green solid curve represents the results for a flat envelope and infinitely long pulse. For the other curves presented, the pulse envelope is sine square with zero carrier-envelope phase, as defined in [5]. The number of optical cycles is $n_p=6$ (black dotted curve), 14 (blue dashed curve), and 22 (red long dashed curve). The curves are shifted by two orders of magnitude with respect to each other for better visibility.

move from even to odd channel closings when the parity of the ground state changes sign.

We have observed two qualitatively different types of enhancements near channel closings: in one case, the enhancement at a given energy as a function of intensity occurs slightly below the nominal CC intensity and is comparatively broad. We referred to this as type I. In contrast, type-II enhancements are extremely sharp, precisely located at the CC intensities, and give rise to sharp peaks in the electron spectrum at energies $E_{\mathbf{p}}=n\omega$ with integer n regardless of the direction of emission. Both types can be attributed to the constructive interference of a large number of long quantum orbits. Type-I enhancements are built up by the superposition of some 20–40 orbits corresponding to ionization up to some 4–8 laser periods before the rescattering event. In contrast, the razor-sharp type-II enhancements require 200 and more orbits to develop fully, corresponding to 50 cycles of the laser field and more.

Figure 18 provides a comprehensive illustration of these observations. It corresponds to Fig. 13 but covers a wider range of parameters. The broad band that moves up from $E_{\mathbf{p}}\approx70$ eV for $n_c=12$ to $E_{\mathbf{p}}\approx150$ eV for $n_c=17$ marks the $10U_P$ cutoff. The further the electron energy moves from the cutoff into the plateau, the more complex becomes the electron yield. In the lower part of the plateau and for higher intensities, we recover the situation of Figs. 2, 7, and 9 where various types of enhancements occur near the same channel closing. The structure of the electron yields generally scales with U_P and therefore moves up in the direction of the diagonal with increasing intensity.

We have also related the enhancements to the well-known threshold anomalies of time-independent (that is, without a

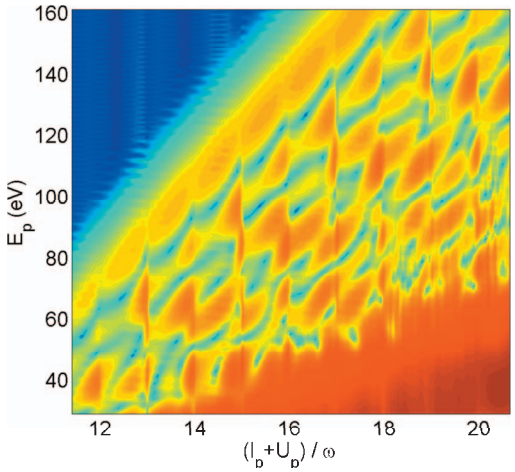

FIG. 18. (Color) Same as Fig. 13, but for a wider range of electron energies and laser intensities.

time-dependent external field) scattering theory, which (for short-range interaction potential) classifies the threshold behavior in four different groups: upward and downward cusps and upward (S-shaped) or downward steps. We have observed only upward cusps and downward rounded steps. Upward cusps correspond to type-II and downward steps to type-I enhancements. For both types, the derivative of the yield at fixed energy with respect to the intensity diverges at the precise CC intensity. For type-II behavior it changes sign at this intensity, which generates the pronounced spike. For type-I, the yield drops steeply at the CC, but whether the drop is infinitely steep (as it actually is) or just very steep makes little difference in a plot of the electron yield. Therefore the notable feature of the type-I yield is not the infinite derivative at the CC, but rather the maximum that precedes it. This maximum, in contrast to the infinite derivative, is already produced by a moderate number of orbits. For high intensity and comparatively low energy, most CCs exhibit enhancements of both types, which can lead to a very complex behavior of the yield.

The CC enhancements have been observed in experiments. In Sec. VIII, by calculating the focal-averaged electron spectra, we have shown that the type-I enhancements may also be observed in the form of peaks in the spectrum which do not appear at $n\omega$ and whose separation is less than ω.

We have found that the enhancements in the photoelectron spectra gradually disappear with the decrease of the laser pulse duration. This is in agreement with the experiments [17,18]. It also confirms our interpretation of these resonant-like enhancements in terms of constructive interference of long orbits.

Finally, we should mention that the improved SFA underlying the calculations as well as the classification of the threshold anomalies is strictly speaking only applicable for short-range potentials and, hence, negative ions. The fact that, notwithstanding, the results bear a lot of similarity with the spectra observed in atoms remains a mystery.

ACKNOWLEDGMENTS

We enjoyed discussions with P. Agostini, S. P. Goreslavski, and G. G. Paulus. Support by the Volkswagen-Stiftung, by the Federal Ministry of Education and Science, Bosnia and Herzegovina, and by the Ministry of Education and Science, Canton Sarajevo, is gratefully acknowledged.

APPENDIX: RESCATTERING *T*-MATRIX ELEMENT FOR SMALL INTERMEDIATE MOMENTA

In this Appendix we derive an expression for the rescattering T-matrix element which is used in Sec. VI in order to show analytically the appearance of the threshold anomalies. We will start from Eq. (10) with Eqs. (9) and (11). For a linearly polarized laser field with the vector potential $\mathbf{A}(t)=\mathbf{A}_0\cos\omega t$, the rescattering matrix element (11) can be written as

$$M_{\mathbf{pk}}^{(0)}(t) = -i\sum_n T_{\mathbf{pk}}^{(0)}(n)\exp[i(E_\mathbf{p}-E_\mathbf{k}-n\omega)t], \tag{A1}$$

where $T_{\mathbf{pk}}^{(0)}(n)=J_n(x)V_{\mathbf{k}-\mathbf{p}}$ is the T-matrix element for laser-assisted potential scattering in the first Born approximation [69]. Here $x=(\mathbf{k}-\mathbf{p})\cdot\mathbf{A}_0/\omega$ and $J_n(x)$ is the ordinary Bessel function of integer order n. Using this result and the relations

$$\int_{-\infty}^{\infty} dt f(t) = \sum_{m=-\infty}^{\infty}\int_0^T dt' f(t'+mT), \tag{A2}$$

$$S_\mathbf{p}(t+T) = S_\mathbf{p}(t) + (E_\mathbf{p}+U_\mathrm{P})T, \tag{A3}$$

and

$$\sum_m \exp(imET) = \omega\sum_m \delta(E-m\omega), \tag{A4}$$

the matrix element $M_{\mathbf{p}i}^{(1)}$, Eq. (10), can be rewritten in the form (12), where the rescattering T-matrix element is given by

$$T_{\mathbf{p}i}^{(1)}(n) = \sum_m \int d^3\mathbf{k} T_{\mathbf{pk}}^{(0)}(m)\int_0^T \frac{dt}{T} M_{\mathbf{k}i}^{(0)}(t) e^{i(E_\mathbf{p}-E_\mathbf{k}-m\omega)t}, \tag{A5}$$

with $E_\mathbf{p}=n\omega-I_\mathrm{P}-U_\mathrm{P}$. The amplitude $M_{\mathbf{k}i}^{(0)}(t)$, Eq. (9), is expressed as an integral over t_0. The integrand contains the quantity

$$\begin{aligned}\mathcal{T}_{\mathbf{k}i}^{(0)}(t_0) &= \langle \mathbf{k}+\mathbf{A}(t_0)|\mathbf{r}\cdot\mathbf{E}(t_0)|\psi_i\rangle e^{i[\mathbf{k}\cdot\boldsymbol{\alpha}(t_0)+\mathcal{U}_1(t_0)]} \\ &= \sum_{n'} T_{\mathbf{k}i}^{(0)}(n')\exp(-in'\omega t_0),\end{aligned} \tag{A6}$$

which is periodic with period $T=2\pi/\omega$. Introducing this into Eq. (A5), taking into account that the integral over t gives $\delta_{m,n-n'}$, and making the substitution $\tau=t-t_0$, we obtain

$$\begin{aligned}T_{\mathbf{p}i}^{(1)}(n) = -i\sum_{n'}&\int d^3\mathbf{k} T_{\mathbf{pk}}^{(0)}(n-n')T_{\mathbf{k}i}^{(0)}(n') \\ &\times\int_0^\infty d\tau e^{-i(E_\mathbf{k}+I_\mathrm{P}+U_\mathrm{P}-n'\omega)\tau}.\end{aligned} \tag{A7}$$

We are interested in the contributions to this integral from small intermediate electron momenta $\mathbf{k}$. Expanding the integrand around $\mathbf{k}=\mathbf{0}$, with the notation $b=I_P+U_P-n'\omega$, we obtain

$$\int_0^\infty d\tau e^{-ib\tau}\int d^3\mathbf{k} f(\mathbf{k})\exp(-i\mathbf{k}^2\tau/2)$$
$$=\int_0^\infty d\tau e^{-ib\tau}\left(\frac{2\pi}{i\tau}\right)^{3/2}\exp\left(-\frac{i}{2\tau}\frac{\partial^2}{\partial\mathbf{k}^2}\right)f(\mathbf{k})|_{\mathbf{k}=\mathbf{0}}$$
$$=-2(2\pi/i)^{3/2}\sqrt{i\pi b}[f(\mathbf{0})-bf''(\mathbf{0})/3+\cdots]. \quad \text{(A8)}$$

Introducing the zeroth-order term of this expansion into Eq. (A7) we get

$$T_{\mathbf{p}i}^{(1)}(n)\approx i(2\pi)^2\sqrt{2\omega}\sum_{n'}T_{\mathbf{p}\mathbf{0}}^{(0)}(n-n')T_{\mathbf{0}i}^{(0)}(n')\sqrt{n'-n_c}, \quad \text{(A9)}$$

where $n_c\equiv(I_P+U_P)/\omega$.

[1] P. Agostini, F. Fabre, G. Mainfray, G. Petite, and N. K. Rahman, Phys. Rev. Lett. **42**, 1127 (1979).
[2] L. F. DiMauro and P. Agostini, Adv. At., Mol., Opt. Phys. **35**, 79 (1995).
[3] W. Becker, F. Grasbon, R. Kopold, D. B. Milošević, G. G. Paulus, and H. Walther, Adv. At., Mol., Opt. Phys. **48**, 35 (2002).
[4] D. B. Milošević and F. Ehlotzky, Adv. At., Mol., Opt. Phys. **49**, 373 (2003).
[5] D. B. Milošević, G. G. Paulus, D. Bauer, and W. Becker, J. Phys. B **39**, R203 (2006).
[6] B. Yang, K. J. Schafer, B. Walker, K. C. Kulander, P. Agostini, and L. F. DiMauro, Phys. Rev. Lett. **71**, 3770 (1993).
[7] K. J. Schafer, B. Yang, L. F. DiMauro, and K. C. Kulander, Phys. Rev. Lett. **70**, 1599 (1993).
[8] G. G. Paulus, W. Nicklich, H. Xu, P. Lambropoulos, and H. Walther, Phys. Rev. Lett. **72**, 2851 (1994); G. G. Paulus, W. Nicklich, and H. Walther, Europhys. Lett. **27**, 267 (1994).
[9] P. B. Corkum, Phys. Rev. Lett. **71**, 1994 (1993).
[10] G. G. Paulus, W. Becker, W. Nicklich, and H. Walther, J. Phys. B **27**, L703 (1994); G. G. Paulus, W. Becker, and H. Walther, Phys. Rev. A **52**, 4043 (1995).
[11] E. Hasović, M. Busuladžić, A. Gazibegović-Busuladžić, D. B. Milošević, and W. Becker, Laser Phys. **17**, 376 (2007).
[12] M. Busuladžić, A. Gazibegović-Busuladžić, and D. B. Milošević, Laser Phys. **16**, 289 (2006).
[13] P. Hansch, M. A. Walker, and L. D. Van Woerkom, Phys. Rev. A **55**, R2535 (1997); M. P. Hertlein, P. H. Bucksbaum, and H. G. Muller, J. Phys. B **30**, L197 (1997).
[14] M. J. Nandor, M. A. Walker, L. D. Van Woerkom, and H. G. Muller, Phys. Rev. A **60**, R1771 (1999).
[15] E. Cormier, D. Garzella, P. Breger, P. Agostini, G. Chériaux, and C. Leblanc, J. Phys. B **34**, L9 (2001).
[16] G. G. Paulus, F. Grasbon, H. Walther, R. Kopold, and W. Becker, Phys. Rev. A **64**, 021401(R) (2001).
[17] F. Grasbon, G. G. Paulus, H. Walther, P. Villoresi, G. Sansone, S. Stagira, M. Nisoli, and S. De Silvestri, Phys. Rev. Lett. **91**, 173003 (2003).
[18] X. Xu, X. Liu, A. A. Kolomenskii, H. A. Schuessler, H. Walther, and G. G. Paulus (to be published).
[19] G. G. Paulus, F. Grasbon, H. Walther, P. Villoresi, M. Nisoli, S. Stagira, E. Priori, and S. De Silvestri, Nature (London) **414**, 182 (2001); D. B. Milošević, G. G. Paulus, and W. Becker, Phys. Rev. Lett. **89**, 153001 (2002); Laser Phys. **13**, 948 (2003).
[20] G. G. Paulus, F. Lindner, H. Walther, A. Baltuška, E. Goulielmakis, M. Lezius, and F. Krausz, Phys. Rev. Lett. **91**, 253004 (2003); D. B. Milošević, G. G. Paulus, and W. Becker, Opt. Express **11**, 1418 (2003); Laser Phys. Lett. **1**, 93 (2004); G. G. Paulus, Laser Phys. **15**, 843 (2005).
[21] D. B. Milošević, G. G. Paulus, and W. Becker, Phys. Rev. A **71**, 061404(R) (2005).
[22] D. B. Milošević and W. Becker, J. Mod. Opt. **52**, 233 (2005); E. Hasović, D. B. Milošević, and W. Becker, Laser Phys. Lett. **3**, 200 (2006).
[23] H. G. Muller and F. C. Kooiman, Phys. Rev. Lett. **81**, 1207 (1998); H. G. Muller, Phys. Rev. A **60**, 1341 (1999); Phys. Rev. Lett. **83**, 3158 (1999); Opt. Express **8**, 44 (2001); **8**, 86 (2001).
[24] R. Wiehle, B. Witzel, H. Helm, and E. Cormier, Phys. Rev. A **67**, 063405 (2003).
[25] J. Wassaf, V. Véniard, R. Taïeb, and A. Maquet, Phys. Rev. Lett. **90**, 013003 (2003); Phys. Rev. A **67**, 053405 (2003).
[26] R. M. Potvliege and S. Vučić, Phys. Rev. A **74**, 023412 (2006); Phys. Scr. **74**, C55 (2006).
[27] R. Bhatt, B. Piraux, and K. Burnett, Phys. Rev. A **37**, 98 (1988).
[28] J. C. Wells, I. Simbotin, and M. Gavrila, Phys. Rev. Lett. **80**, 3479 (1998).
[29] R. Kopold, W. Becker, M. Kleber, and G. G. Paulus, J. Phys. B **35**, 217 (2002).
[30] S. V. Popruzhenko, Ph. A. Korneev, S. P. Goreslavski, and W. Becker, Phys. Rev. Lett. **89**, 023001 (2002).
[31] M. Lewenstein, Ph. Balcou, M. Yu. Ivanov, A. L'Huillier, and P. B. Corkum, Phys. Rev. A **49**, 2117 (1994).
[32] R. Kopold, W. Becker, and M. Kleber, Opt. Commun. **179**, 39 (2000).
[33] R. Kopold, D. B. Milošević, and W. Becker, Phys. Rev. Lett. **84**, 3831 (2000).
[34] P. Salières, B. Carré, L. Le Déroff, F. Grasbon, G. G. Paulus, H. Walther, R. Kopold, W. Becker, D. B. Milošević, A. Sanpera, and M. Lewenstein, Science **292**, 902 (2001).
[35] C. Figueira de Morisson Faria, H. Schomerus, and W. Becker, Phys. Rev. A **66**, 043413 (2002).
[36] D. B. Milošević and W. Becker, Phys. Rev. A **66**, 063417 (2002); S. Odžak and D. B. Milošević, *ibid.* **72**, 033407

(2005).
[37] D. B. Milošević, D. Bauer, and W. Becker, J. Mod. Opt. **53**, 125 (2006).
[38] E. P. Wigner, Phys. Rev. **73**, 1002 (1948).
[39] L. D. Landau and E. M. Lifshitz, *Quantum Mechanics* (Pergamon, Oxford, 1977), Sec. 417.
[40] A. I. Baz', Ya. B. Zel'dovich, and A. M. Perelomov, *Scattering, Reactions and Decays in Nonrelativistic Quantum Mechanics* (Nauka, Moscow, 1971), Sec. IX.
[41] A. I. Baz', Zh. Eksp. Teor. Fiz. **33**, 923 (1957) [Sov. Phys. JETP **6**, 709 (1958)].
[42] R. G. Newton, Ann. Phys. (N.Y.) **4**, 29 (1958).
[43] R. G. Newton, *Scattering Theory of Waves and Particles*, 2nd ed. (Springer, New York, 1982).
[44] F. H. M. Faisal and P. Scanzano, Phys. Rev. Lett. **68**, 2909 (1992).
[45] B. Borca, M. V. Frolov, N. L. Manakov, and A. F. Starace, Phys. Rev. Lett. **88**, 193001 (2002); B. Borca, A. F. Starace, A. V. Flegel, M. V. Frolov, and N. L. Manakov, Phys. Rev. A **65**, 051402(R) (2002).
[46] M. V. Frolov, N. L. Manakov, E. A. Pronin, and A. F. Starace, Phys. Rev. Lett. **91**, 053003 (2003); J. Phys. B **36**, L419 (2003).
[47] N. L. Manakov and M. V. Frolov, Pis'ma Zh. Eksp. Teor. Fiz. **83**, 630 (2006) [JETP Lett. **83**, 536 (2006)].
[48] K. Krajewska, I. I. Fabrikant, and A. F. Starace, Phys. Rev. A **74**, 053407 (2006); Laser Phys. **17**, 368 (2007).
[49] K. Krajewska, I. I. Fabrikant, and A. F. Starace, Bull. Am. Phys. Soc. **51**, 119 (2006).
[50] For limitations of this approach, see, for example, M. V. Frolov, A. A. Khuskivadze, N. L. Manakov, and A. F. Starace, J. Phys. B **39**, S283 (2006).
[51] W. Becker, A. Lohr, and M. Kleber, J. Phys. B **27**, L325 (1994); **28**, 1931 (1995); A. Lohr, M. Kleber, R. Kopold, and W. Becker, Phys. Rev. A **55**, R4003 (1997).
[52] M. Lewenstein, K. C. Kulander, K. J. Schafer, and P. H. Bucksbaum, Phys. Rev. A **51**, 1495 (1995).
[53] D. B. Milošević and F. Ehlotzky, Phys. Rev. A **57**, 5002 (1998); **58**, 3124 (1998); J. Phys. B **32**, 1585 (1999).
[54] S. P. Goreslavskii and S. V. Popruzhenko, Phys. Lett. A **249**, 477 (1998).
[55] D. B. Milošević, A. Gazibegović-Busuladžić, and W. Becker, Phys. Rev. A **68**, 050702(R) (2003); A. Gazibegović-Busuladžić, D. B. Milošević, and W. Becker, *ibid.* **70**, 053403 (2004).
[56] N. Bleistein and R. A. Handelsman, *Asymptotic Expansions of Integrals* (Dover, New York, 1986).
[57] A similar classification for the high-order above-threshold ionization process was presented in Ref. [30], and for high-order harmonic generation in Ref. [58].
[58] L. E. Chipperfield, L. N. Gaier, P. L. Knight, J. P. Marangos, and J. W. G. Tisch, J. Mod. Opt. **52**, 243 (2005).
[59] In the Lewenstein model, with few exceptions only the shortest two orbits are considered. In our nomenclature, these are the orbits $(\alpha\beta m)=(1-10)$ and $(-1-10)$. The former has the shorter travel time and is, in the literature, frequently called the "short orbit," latter has a longer travel time and is called the "long orbit."
[60] L. V. Keldysh, Zh. Eksp. Teor. Fiz. **47**, 1945 (1964) [Sov. Phys. JETP **20**, 1307 (1965)].
[61] Contrary to high-order harmonic generation, where two sets of solutions $\{\varphi_0,\varphi\}$, and $\{\varphi_0+\alpha\pi,\varphi+\alpha\pi\}$, lead to the emission of only odd harmonics [36], for high-order ATI we have only one set of solutions.
[62] V. A. Borovikov, *Uniform Stationary Phase Method* (The Institution of Electrical Engineers, London, 1994).
[63] A. Čerkić and D. B. Milošević, Phys. Rev. A **73**, 033413 (2006).
[64] N. L. Manakov, A. F. Starace, A. V. Flegel, and M. V. Frolov, JETP Lett. **76**, 258 (2002).
[65] A. Čerkić and D. B. Milošević, Phys. Rev. A **70**, 053402 (2004); Laser Phys. **15**, 268 (2005).
[66] L. Fonda, Nuovo Cimento, Suppl. **20**, 116 (1961).
[67] L. Fonda and R. G. Newton, Ann. Phys. (N.Y.) **7**, 133 (1959).
[68] M. Gailitis, Zh. Eksp. Teor. Fiz. **44**, 1974 (1963) [Sov. Phys. JETP **17**, 1328 (1963)].
[69] F. V. Bunkin and M. V. Fedorov, Zh. Eksp. Teor. Fiz. **49**, 1215 (1965) [Sov. Phys. JETP **22**, 844 (1965)].